

The contribution of synchrotron X-ray computed microtomography to understanding volcanic processes

Margherita Polacci,^{a*} Lucia Mancini^b and Don R. Baker^{c,d}

^aIstituto Nazionale di Geofisica e Vulcanologia, Sezione di Pisa, via della Faggiola 32, 56126 Pisa, Italy, ^bSYRMEP Group, Sincrotrone Trieste SCpA, SS 14, Km 163, 5 in Area Science Park, 34012 Basovizza (Trieste), Italy, ^cEarth and Planetary Sciences, McGill University, GEOTOP-UQUAM-McGill Research Centre, 3450 rue University, Montreal, QC H3A2A7, Canada, and ^dSincrotrone Trieste SCpA, SS 14, Km 163, 5 in Area Science Park, 34012 Basovizza (Trieste), Italy.
E-mail: polacci@pi.ingv.it

A series of computed microtomography experiments are reported which were performed by using a third-generation synchrotron radiation source on volcanic rocks from various active hazardous volcanoes in Italy and other volcanic areas in the world. The applied technique allowed the internal structure of the investigated material to be accurately imaged at the micrometre scale and three-dimensional views of the investigated samples to be produced as well as three-dimensional quantitative measurements of textural features. The geometry of the vesicle (gas-filled void) network in volcanic products of both basaltic and trachytic compositions were particularly focused on, as vesicle textures are directly linked to the dynamics of volcano degassing. This investigation provided novel insights into modes of gas exsolution, transport and loss in magmas that were not recognized in previous studies using solely conventional two-dimensional imaging techniques. The results of this study are important to understanding the behaviour of volcanoes and can be combined with other geosciences disciplines to forecast their future activity.

1. Introduction

Volcanoes are complex systems that require the integration of many different scientific disciplines to understand their behaviour and to monitor and forecast their activity. The generalized model of volcanic eruption mechanisms is that magma at high pressure (depths of many kilometres below the surface) contains weight percent (up to ~6 wt%) concentrations of dissolved volatiles, particularly water. As these magmas ascend they become supersaturated (because of the positive dependence of water solubility with pressure) and a separate gas phase exsolves (for a review on this topic see Carroll & Holloway, 1994; Oppenheimer *et al.*, 2003). If this gas phase can be slowly released to the surrounding rocks or atmosphere the volcanic activity is minor; however, if this gas phase remains trapped as bubbles in the magma the potential for a hazardous volcanic eruption increases significantly. Thus, volcanic processes intimately depend upon the rates and mechanisms of gas exsolution into bubbles and the loss of gas to the country rocks or outside the volcanic crater. Because volcanic rocks cool quickly when ejected, the bubbles formed by the exsolved gas are quenched into the solidified rock

texture even though they have lost their original gas. These former gas bubbles, now voids in the rock samples, are named vesicles (Cashman & Mangan, 1994).

Indeed, textures of volcanic rocks have proved to provide important constraints on processes occurring in magma chambers (*e.g.* Jerram & Martin, 2008), volcanic conduits (Polacci *et al.*, 2001; Houghton *et al.*, 2004) and during lava emplacement on volcano flanks (Cashman *et al.*, 1994; Gaonac'h *et al.*, 1996a). For example, crystal and vesicle textures bear the fingerprints of processes related to permeability (Rust & Cashman, 2004; Bouvet de Maissonneuve *et al.*, 2008; Wright *et al.*, 2009), gas transport (Burton *et al.*, 2007) and fragmentation (Klug *et al.*, 2002; Polacci *et al.*, 2003) in magmas and can be used as a proxy to investigate such processes. The classical approach to studying textures of erupted products is to acquire two-dimension (2-D) images of volcanic samples *via* optical and/or scanning electron microscopy on areal sections (*i.e.* thin sections) (Cashman & Mangan, 1994; Higgins, 2006). An advantage of this procedure is that it offers a fast quantitative inspection of volcanic textures in 2-D, which can be very useful in the short time usually involved with eruption monitoring and civil protection

Table 1

Summary of information on the volcanic rocks displayed in Fig. 4.

Sample	Type	Composition	Volcano (crater)	Eruptive style	Vesicularity	VND† (mm ⁻³)
Str240506b	Scoria	HK‡ basalt	Stromboli (North-East crater)	Strombolian	0.49	2 × 10 ²
Str50403	Pumice	HK‡ basalt	Stromboli (summit craters)	Paroxysmal Strombolian	0.57	6 × 10 ²
ET201006c	Scoria	Alkaline basalt	Etna (South-East crater)	Strombolian	0.72	1 × 10 ²
BBSC9	Scoria	Tholeiitic basalt	Ambrym (Benbow crater)	Violent Strombolian	0.59	1 × 10 ³
UM1MN4top	Scoria	Trachyte	Campi Flegrei (Monte Nuovo crater)	Vulcanian	0.46	1 × 10 ³
LMMN2C2	Pumice	Trachyte	Campi Flegrei (Monte Nuovo crater)	Vulcanian	0.38	1 × 10 ³

† VND stands for vesicle number density. ‡ HK stands for high potassium.

planning. However, because it provides no direct information in the third dimension, this approach cannot be used to investigate the true internal structure of volcanic materials, limiting the information that can be provided on vesiculation, degassing and crystallization processes, as well as on the overall eruption dynamics. Recently, the application of X-ray computed microtomography (μ CT) to geological specimens (Song *et al.*, 2001; Ketcham *et al.*, 2005; Gualda & Rivers, 2006; Polacci *et al.*, 2006) has opened the opportunity to completely visualize and quantify the internal structure of porous materials, such as volcanic scoria and pumice clasts, directly in three dimensions. In this framework, a few years ago we started a project with the goal of performing X-ray microtomographic analysis and reconstructing three-dimensional (3-D) digital volumes of volcanic specimens. In this paper we first discuss how we reconstructed and quantitatively processed 3-D textural features in volcanic products from explosive activity of several different active hazardous volcanic areas in Italy and other parts of the world: Stromboli (Aeolian Archipelago, Italy), Mount Etna (Eastern Sicily, Italy), Campi Flegrei (Neapolitan area, Southern Italy), Villarrica (Chile) and Ambrym (Vanuatu Islands). We then provide examples of the comparison between 2-D and 3-D data and describe how we used the 3-D dataset to constrain the dynamics of vesiculation and degassing in basaltic and trachytic magmas.

2. Materials and methods

Our sample suite comprises more than 60 vesicle-bearing volcanic rocks of the lapilli size (generally between 1 and 3 cm). Such samples were specifically selected for this study because they do not contain post-eruptive textural features and can therefore be assumed representative of the state of magma within the conduit before the eruption, providing important information on volcanic processes. In detail, the analyzed samples can be subdivided into two categories. The first one concerns samples of basaltic ($\text{SiO}_2 = 45\text{--}52$ wt%) composition and erupted from persistently degassing volcanoes characterized by mild to moderate explosive activity. This category includes (i) scoria clasts from the 2006 autumn Mount Etna eruption, (ii) scoria clasts from the normal Strombolian activity at Stromboli and collected between March 2004 and May 2006, (iii) pumice clasts from the much more dangerous 5 April 2003 and 15 March 2007 paroxysmal explosions at Stromboli, (iv) scoria clasts from activity at Villarrica in November 2004 and scoria clasts collected at

Ambrym in October 2008 and belonging to previous explosive activity of the Benbow crater (refer to Barberi *et al.*, 1993; Robin *et al.*, 1993; Bertagnini *et al.*, 2003; Behncke *et al.*, 2006; Gurioli *et al.*, 2008 and references therein for information about these volcanoes and their eruptive activity). The second category refers to pumice clasts of trachytic ($\text{SiO}_2 = \sim 58\text{--}69$ wt%, $\text{Na}_2\text{O} + \text{K}_2\text{O} = >\sim 7$ wt%) composition that were collected from deposits left by explosive activity that occurred at Campi Flegrei, an active caldera situated west of the urban centre of Naples, Italy. These samples belong to three historical eruptions that involved three different vents/points of magma emission characterized by highly to moderately explosive (Plinian to Sub-Plinian to Vulcanian) eruptive style: the Campanian Ignimbrite (39 k-years), Agnano Monte Spina (4.1 k-years) and Monte Nuovo (AD 1538), reported here in order of decreasing eruptive intensities (refer to Piochi *et al.*, 2008 and references therein for information about these eruptions). Table 1 summarizes information related to the six volcanic rocks displayed in Fig. 4 that were chosen as representative of the two sample categories described above.

The microtomographic experiments were performed at the SYRMEP beamline of the Elettra synchrotron radiation facility in Basovizza (Trieste, Italy). This beamline is very well suited for investigations on volcanic rocks because of the high photon flux, the energy range available, the beam geometry and the achievable spatial resolution. The X-ray source is one of the bending magnets of Elettra and the beamline provides, at a distance of about 23 m from the source, a monochromatic laminar-section X-ray beam with a maximum area of about 160 mm × 6 mm. The monochromator, which covers the entire angular acceptance of the beamline, is based on a double-Si(111) crystal system working in Bragg configuration and the energy of the X-ray beam can be tuned between 8.3 and 35 keV with an energy-resolving power of $\sim 10^{-3}$. Owing to the small source size, the source-to-sample distance and the simple optical design of the SYRMEP beamline, the X-ray beam is characterized by a high spatial coherence (the transversal coherence length is about 10 μm at 15 keV) that allows phase-contrast (PhC) imaging to be performed with a simple experimental set-up (reported in Fig. 1). In fact, in the case of third-generation sources, PhC imaging is based on free-space propagation: contrary to the absorption mode where the sample is kept very close to the detector, in PhC mode the sample-to-detector distance d usually varies between 10 and 100 cm. The X-rays exiting from the sample propagate in the free space until they reach the detector. Free-space propaga-

tion transforms the phase modulation of the transmitted beam into amplitude modulation and the contrast is originated from interference among parts of the wavefronts that have experienced different phase shifts (Fresnel diffraction). According to the choice of d with respect to the size a of the features to be identified perpendicularly to the beam direction, one may discriminate between two regimes: the edge detection regime ($d \ll a^2/\lambda$ where λ is the X-ray wavelength) and the holography regime ($d \simeq a^2/\lambda$). The produced diffraction pattern appears superimposed on the conventional absorption pattern on the detector and the net effect is an enhanced visibility of the edges of the sample features such as inclusions, pores and interfaces between regions with different mass density. In the edge detection regime the microtomographic images can be used directly to extract morphological information from the analyzed sample (Snigirev *et al.*, 1995; Cloetens *et al.*, 1996). By using PhC microtomography we were able to visualize small variations in density and chemical composition and to image different phases in the rock (such as crystals, vesicles and the matrix), owing to the contrast enhancement at their boundaries (Mancini *et al.*, 1998). In addition, the use of a monochromatic parallel X-ray beam resulted in a more precise definition of the vesicle outlines with respect to conventional sources, avoiding beam artefacts such as beam hardening and image magnification. Finally, a synchrotron radiation source allows us to dramatically improve the signal-to-noise ratio compared with a conventional X-ray tube (Baruchel *et al.*, 2000). This allowed us to perform highly precise quantitative analyses of vesicles in the samples. More details on the experimental set-up of the SYRMEP beamline can be found at <http://www.elettra.trieste.it/experiments/beamlines/syrmep/> as well as in Polacci *et al.* (2006, 2009).

During acquisition of tomographic scans each sample was mounted on a high-resolution rotation stage and rotated with equi-angular separation between 0 and 180° (Fig. 1). A water-cooled CCD camera was used as detector. The camera head consists of a high-resolution full-frame CCD imager, which is

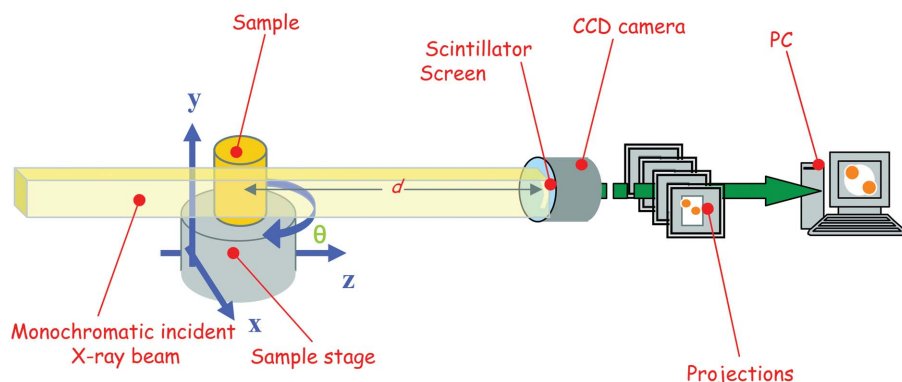


Figure 1

Sketch of the experimental set-up for microtomography experiments at the SYRMEP beamline of Elettra.

Table 2

Summary of the experimental conditions for the volcanic rocks described in Table 1.

Sample	Detector configuration	Energy (keV)	Number of projections	Sample-to-detector distance (mm)	Pixel size (μm)	Binning
Str240506b	(II)	28	900	200	9	2×2
Str50403	(III)	27	720	120	14	1×1
ET201006c	(II)	30	900	200	9	2×2
BBSC9	(II)	28	1200	200	9	2×2
UM1MN4top	(II)	25	900	80	4.5	1×1
LMMN2C2	(II)	25	900	80	4.5	1×1

directly bonded to a tapered fibre optic. A GadOx scintillator screen has been deposited directly onto the front surface of this tapered fibre optic. For the different types of samples the sample-to-detector distance was chosen in order to work in the edge-detection regime for PhC microtomography (Cloetens *et al.*, 1996).

The investigated samples were approximately cut into parallelepipeds with a square base of about $5 \text{ mm} \times 5 \text{ mm}$ and a height of between 10 and 20 mm. In order to be able to examine the broadest possible range of sample textures, three different detector configurations available at SYRMEP were used. In configuration (I) samples were imaged by using a 16-bit, 2048×2048 pixel, Photonics Science Hystar CCD camera with an effective pixel size of $3.85 \mu\text{m}$ and a field of view of $8 \text{ mm} \times 8 \text{ mm}$; in configuration (II) samples were imaged using a 12-bit, 4008×2672 pixel, Photonics Science XDI-VHR CCD camera with an effective pixel size of $4.5 \mu\text{m}$ and a field of view of $18 \text{ mm} \times 12 \text{ mm}$; finally in configuration (III) samples were analyzed by a 16-bit, 2048×2048 pixel, Photonics Science Hystar CCD camera with a pixel size of $14 \mu\text{m}$ and a field of view of $28 \text{ mm} \times 28 \text{ mm}$. Configurations (I) and (II) at binning 1×1 were used to image pyroclastic products from Campi Flegrei because these rocks had the finest structure and therefore required the highest resolution possible. Configuration (II) at binning 2×2 and configuration (III) were instead used for the rest of our sample suite. Table 2 reports details of the experimental conditions used for the samples described in Table 1.

Depending upon the selected detector configuration and the sample size (Kak & Slaney, 1988), between 720 and 1800 projections were collected for each tomographic scan (see Table 2). Tomographic scans lasted from less than 1 h to a maximum of 5 h depending on the ring current, sample absorption, pixel size of the detector and number of projections. The tomographic projections were reconstructed into 2-D slices using the *Syrmep_tomo_project* software custom-developed in IDL language by the SYRMEP group (for details see Mancini *et al.*, 2003) and based on the filtered backprojection algorithm (Herman, 1980; Kak & Slaney, 1988). The reconstructed slices were then stacked using the freeware

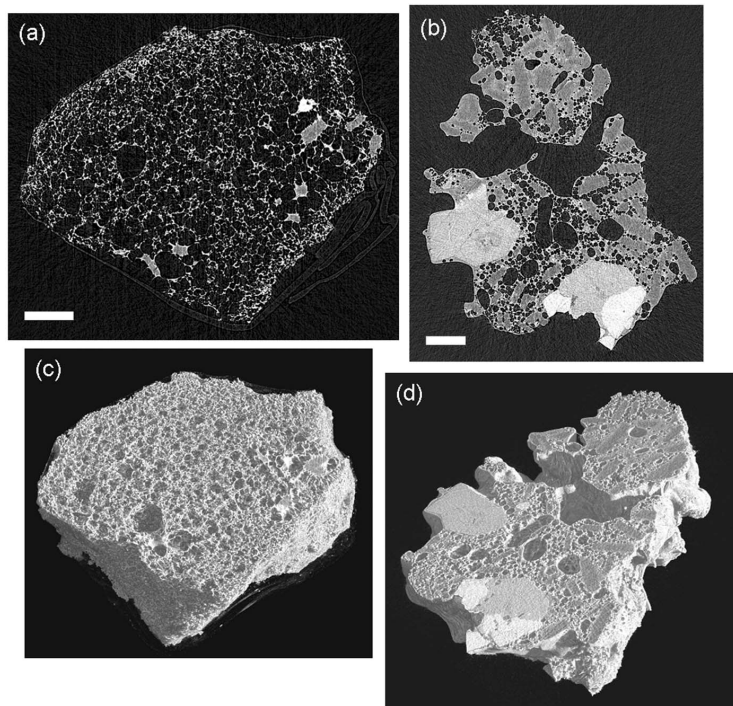


Figure 2
Reconstructed slices of fine pumice structure (a) and coarse scoria texture (b) in volcanic rocks from Stromboli volcano (Italy). In both images black voids are vesicles, dark and light grey and white objects are crystals, the matrix (glass + fine crystals) is intermediate grey, and the scale bar is 1 mm. (c) and (d) are volume renderings of the samples in (a) and (b), respectively. Pixel size = 9 μm. See text for further details.

ImageJ software (Abramoff *et al.*, 2004) for visualizing the internal structure of the porous volcanic rocks. The resulting 3-D digital volumes (Fig. 2) were rendered using the commercial software *VGStudio MAX 2.0*. Because we were interested in magma vesiculation and degassing, quantitative 3-D measurements were only devoted to vesicle textures. The 3-D digital volumes were processed using the *Blob3D* software for 3-D image analysis, as fully described by Ketcham (2005). After manual vesicle segmentation by simple greyscale thresholding, and vesicle separation following one or more erosion and dilation cycles to separate impinging but not coalescing vesicles, vesicles were counted using the same software. The individual vesicle volumes were then used in each sample for calculating several textural parameters, such as vesicularity (calculated as the sum of all vesicle volumes/total volume of sample), vesicle number density (defined here as the total number of vesicles normalized to the bulk volume in each sample) (Table 1), and vesicle volume distributions (Figs. 3b and 3d).

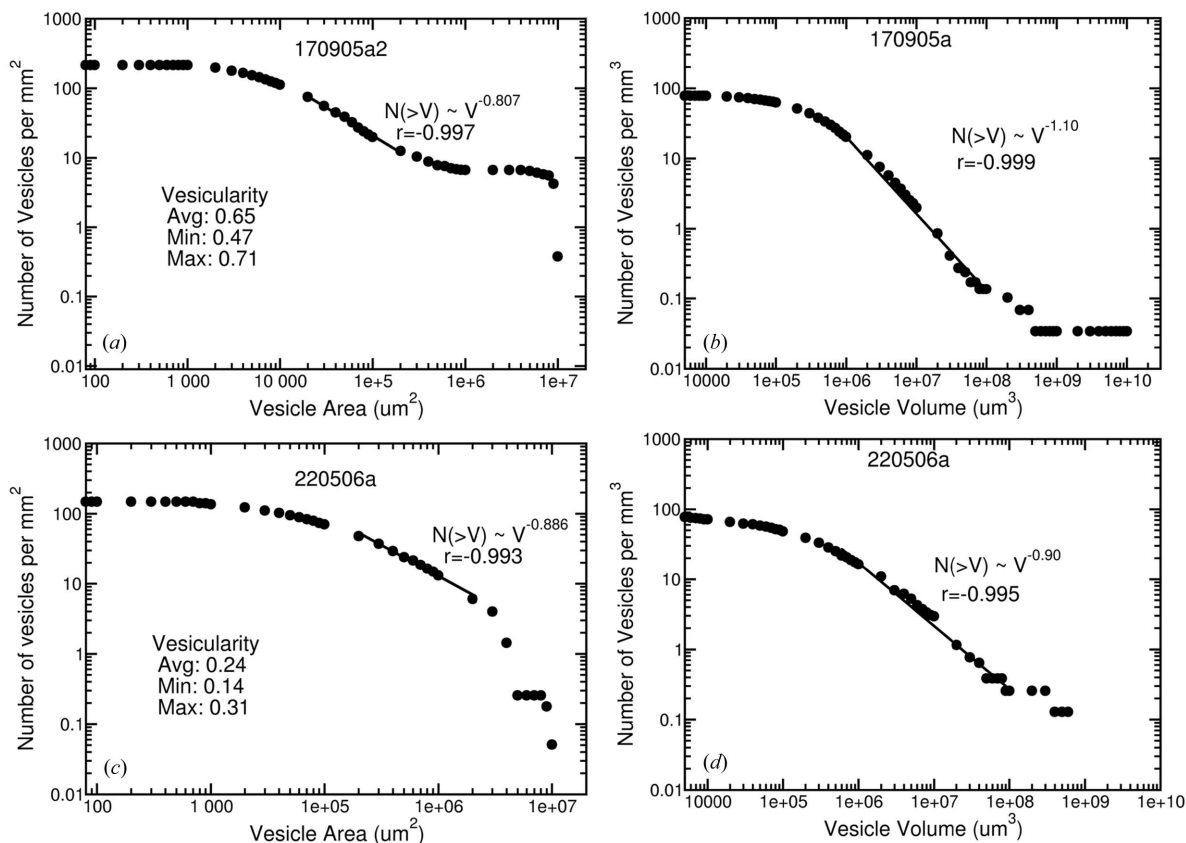


Figure 3
Comparison between 2-D [(a) and (c)] and 3-D [(b) and (d)] cumulative vesicle size distributions for basaltic scoria samples 170905a and 220506b erupted from normal explosions at Stromboli. See text for further explanations.

3. Results and discussion

3.1. 2-D versus 3-D measurements of volcanic rock textures

3-D views of volcanic rock textures provided us with the unprecedented opportunity to investigate textural features that cannot be unambiguously recognized in 2-D sections where they can potentially lead to incorrect interpretations. Here we offer two examples of the comparison between the vesicle size distributions (expressed both in area and in volume) of two scoria clasts from the normal explosive activity of Stromboli using 2-D images and 3-D X-ray μ CT. For both (2-D and 3-D) sets of data, distributions are displayed on a cumulative basis in a log–log plot and can be fit by a power law with an exponent close to 1. In the volcanological literature, power laws with an exponent of ~ 1 are common and have been interpreted as resulting from either vesicle coalescence (Gaonac'h *et al.*, 1996a,b), continuous vesicle nucleation (Blower *et al.*, 2002) or a combination of both processes (Polacci *et al.*, 2009). Power law distributions and their exponents are therefore an important tool in providing information on magma vesiculation and related processes.

The vesicle size distributions presented here display small but significant differences between them (Fig. 3). The most important difference in sample 170205a is that the 2-D data (Fig. 3a) do not indicate the presence of the one large vesicle seen in the 3-D distribution (Fig. 3b); instead they indicate the

presence of many large, yet smaller in comparison with the 3-D large one, isolated vesicles. The shapes of the large vesicles, as the one illustrated in Fig. 3(b), are so convoluted (see example of 3-D large vesicles in scoria clast, Fig. 4a) that there is no rigorous method for the conversion of the 2-D results to 3-D. A second difference (Fig. 3a) is the appearance of a region of intermediate-to-large vesicle sizes in the 2-D data between 10^4 and $10^6 \mu\text{m}^2$ that follows a power law with a 3-D exponent (calculated on the basis of the 2-D exponent, as suggested by Gaonac'h *et al.*, 1996b) different from that of intermediate-to-large vesicles in the 3-D results (Fig. 3b). Such a slope could easily lead to an incorrect interpretation of the 2-D data. Finally, the sample vesicularity varies between 0.47 and 0.71 with an average of 0.65; if only a few slices of this sample were measured, the measured vesicularity could conceivably have been in error.

The spectacular difference between the 2-D and 3-D distributions of sample 220506a is the lack of an obvious power law in the 2-D data and its presence in 3-D (Figs. 3c and 3d). However, a power law can be fit to the 2-D data (Fig. 3c), but we only did so because of our knowledge of the 3-D results (Fig. 3d). Also, the 2-D data demonstrate a more precipitous drop in the concentration of the large vesicles than actually seen in 3-D. Finally, the variation in vesicularity of this sample is so great that if only a few slices were investigated it is unlikely that the true vesicularity would be known.

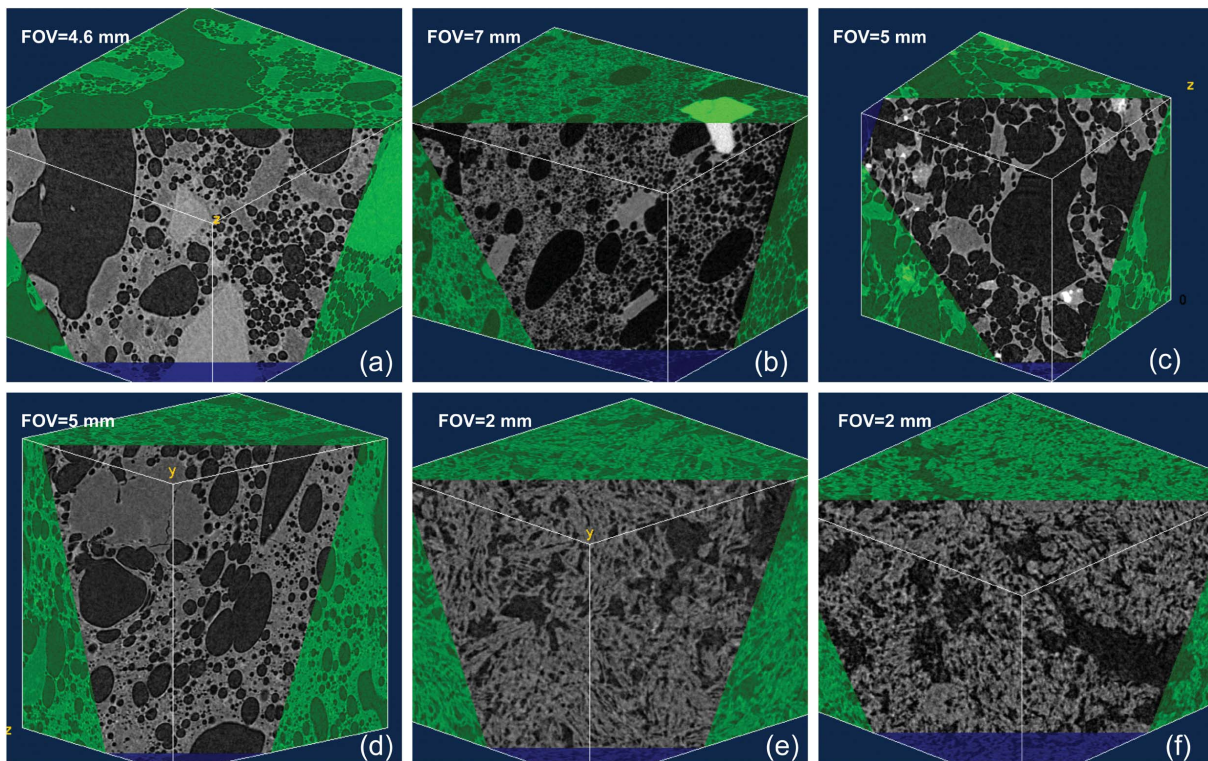


Figure 4

3-D views of volcanic rocks from explosive eruptions. The cutting plane (in greyscale) displays internal clast textures. Sample labels in parentheses as reported in Table 1. From the top left, (a) basaltic scoria (Str240506b) from normal explosive activity at Stromboli, (b) pumice (Str50403) from paroxysmal explosive activity at Stromboli, (c) scoria (ET201006c) from Mount Etna explosive activity in October 2006, (d) scoria (BBSC9) from the explosive activity of Ambrym (Vanuatu Islands), (e) trachytic scoria (UM1MN4top) and (f) pumice (LMMN2C2) from the Monte Nuovo explosive eruption in AD 1538 (Campi Flegrei caldera). See text for further explanations. In all 3-D views black voids are vesicles, dark and light grey and white objects are crystals and the matrix is intermediate grey. FOV stands for field of view.

3.2. 3-D characterization of volcanic rock textures

μ CT using a synchrotron X-ray source provides us with the ability to accurately reconstruct the real crystal and vesicle textures present in volcanic specimens. We describe here a series of examples of 3-D views of the volcanic rocks that we have investigated at the SYRMEP beamline during the past few years, particularly focusing on vesicle textures (Fig. 4). We start with a comparison between the textures of basaltic scoria (crystal-bearing vesicular lapilli) (Fig. 4a) and pumice (almost crystal-free vesicular lapilli) (Fig. 4b) clasts from normal and paroxysmal explosive activity at Stromboli, the volcano for which we have the largest number of samples investigated *via* X-ray μ CT and the most exhaustive set of quantitative measurements. The normal volcanic activity of Stromboli is characterized by mild to moderate explosions occurring between 4 and 30 times per hour; this activity has been occurring since at least Roman times (Barberi *et al.*, 1993). However, occasionally these small eruptions stop and this repose is broken by a much larger paroxysmal eruption (Barberi *et al.*, 1993) that poses a significant hazard to the population of the island.

Scoriae from normal Strombolian explosions contain volume fractions of crystals that can exceed 0.40, and a vesicularity that varies from 0.24 to 0.80. The sample reported here (Str240506b) has a vesicularity of 0.49 and a number density of $2 \times 10^2 \text{ mm}^{-3}$ (Table 1) and nicely illustrates the occurrence of two vesicle populations, one of the defining features of these basaltic scoria textures. The first population consists of large, irregularly shaped and well interconnected vesicles between $\sim 500 \mu\text{m}$ to a few millimetres in size; the second is made of small-to-intermediate ($< 100 \mu\text{m}$ – $500 \mu\text{m}$) spherical to subspherical vesicles occupying the space between crystals and the larger vesicles (Fig. 4a). The two populations can be clearly seen in the 3-D vesicle size distributions of Figs. 3(b) and 3(d), the former being illustrated by the plateau at the end of the distribution and the latter by the vesicle subpopulation that describes a distribution fit by a power law with an exponent of ~ 1 . Pumice clasts from paroxysmal explosions at Stromboli have a much finer structure in comparison with scoria textures. The pumice sample (Str50403) illustrated in Fig. 4(b) was erupted during the 5 April 2003 paroxysm. It is poorly crystalline (crystal volume fraction < 0.05), has a vesicularity of 0.57 and a vesicle number density of $6 \times 10^2 \text{ mm}^{-3}$ (Table 1). Its internal structure consists of a network of small-to-intermediate spherical vesicles ($\sim \leq 200 \mu\text{m}$) and larger ellipsoidal vesicles scattered throughout the investigated sample volume. 3-D views, however, reveal that these latter vesicles are not well interconnected and do not form a network of coalescing objects that span the entire volume under investigation, as we found in the scoria clasts erupted during normal explosive activity from the same volcano.

Our second case study compares the textures of two basaltic scoria clasts erupted from the mild to moderate explosive activity (similar to the normal activity described for Stromboli) of Mount Etna (Fig. 4c) and Ambrym (Fig. 4d) volca-

noes. The Etna sample (ET201006c) has a vesicularity of 0.72 and vesicle number density of $1 \times 10^2 \text{ mm}^{-3}$ (Table 1). It contains large interconnected vesicles with complex shapes and smaller spherical to subspherical vesicles, displaying two vesicle populations similar in size and texture to those found in the Stromboli scoria clast described above. In the Ambrym sample (BBSC9), the largest vesicles ($\sim \geq 1 \text{ mm}$) fall into two morphological categories: subspherical and isolated vesicles and irregularly shaped and interconnected ones (Fig. 4d). We observe that the small to intermediate vesicles are more deformed than in the Stromboli scoria. This is particularly visible in the flattened vesicles around large subspherical vesicles (see the large vesicle in the centre-left part of Fig. 4d). As a final example for this study, we have chosen to illustrate the scoria (UM1MN4top) (Fig. 4e) and pumice (LMMN2C2) (Fig. 4f) clasts erupted during the AD 1538 Monte Nuovo eruption. The products of this eruption are interesting to compare with the basaltic products presented above because they were generated by magmas of trachytic composition (*i.e.* more compositionally evolved than basaltic magmas) and the eruption was characterized by a longer duration and higher magma explosivity than basaltic explosions. As a result, the textural features exhibited by these rocks are remarkably different in comparison with those found in the pyroclastic material erupted from Stromboli, Mount Etna or Ambrym. Besides overall higher vesicle number densities ($1 \times 10^3 \text{ mm}^{-3}$, Table 1), the most obvious difference lies in the crystal sizes and in the shape and spatial arrangement of vesicle textures. While basaltic samples generally have millimetre-sized crystals, in the trachytic samples crystals are mostly feldspars less than $100 \mu\text{m}$ in size; vesicles ($< 100 \mu\text{m}$ to millimetres in size) occupy the voids left by the crystal framework and display very irregular shapes (Fig. 4e). In both pumice and scoria such irregularly shaped vesicles generate micro-crack-like vesicle paths (see vesicle path from bottom right to top left in Fig. 4f) given by a network of interconnected individuals spanning the whole volume under investigation. These vesicle paths differ from those developed by the Stromboli samples, that more closely resemble channel-like vesicle pathways (as, for example, the large vesicle at left of Fig. 4a).

3.3. Interpretation of 3-D textures

The results of the present study allow us to shed light on processes occurring in volcanic conduits and accompanying gas and magma ascent to the Earth's surface. For example, the large interconnected vesicles in basaltic scoria clasts have been interpreted as percolation pathways for most gas to flow non-explosively to the volcanic vent of persistently degassing basaltic volcanoes. The fact that such vesicles have been found in products erupted from several active basaltic volcanoes (such as Stromboli, Mount Etna and Ambrym) located in different tectonic settings and characterized by different and variable eruptive intensity strongly suggests that basaltic systems appear to follow a common degassing pathway. However, not all explosive basaltic rocks contain large

coalescing vesicles. Pumice clasts from the much more violent, dangerous and less frequent paroxysmal explosions at Stromboli do not present this type of vesicle, demonstrating that basaltic volcanoes develop different vesicle textures and therefore degassing dynamics with increasing explosive activity (Polacci *et al.*, 2009).

Large interconnected vesicles that form micro-cracks are also found in the trachytic material from the Monte Nuovo eruption. Although by their shape micro-crack-like vesicles might appear to be less efficient in transporting gas than channel-like vesicles, this textural evidence suggests that gas was percolating in the Monte Nuovo conduit system before the eruption and that open-system degassing may be an effective way through which gas is lost at the crater surface in some explosive trachytic eruptions at Campi Flegrei, leading to only moderately violent activity as in the case of the Monte Nuovo eruption. Had the samples (*i.e.* the magma) not contained the micro-crack vesicle network, we point out that the explosive activity would have been much more violent.

4. Concluding remarks

Our findings highlight that synchrotron radiation X-ray μ CT is a powerful tool in investigating rock textures because it offers us the unprecedented ability to detail the geometry of vesicles and crystals directly in 3-D and to visualize textural features that are not possible to recognize unambiguously in 2-D areal sections of the same rocks. Work in progress consists of establishing an optimized protocol that will enable us to quantitatively study the 3-D texture of different types of rocks and their composition in a statistically representative way. Future work will concentrate on the study of the spatial relations between phases (crystals, vesicles and matrix) in rocks and their implications on the rheological properties of magmas and on the intensity of explosive activity at volcanoes.

We thank Franco Zanini, Giuliana Tromba, Stefano Favretto, Nicola Sodini, Diego Dreossi, Liping Bai and Livia Colò for help during acquisition of tomographic scans. We also thank Monica Piochi, Daniele Andronico, Mauro Rosi, Alessandro La Spina and Filippo Murè for collecting some of the rock samples investigated in this study. Marco Voltolini is gratefully acknowledged for providing an informal review of the manuscript.

References

- Abramoff, M. D., Magelhaes, P. J. & Ram, S. J. (2004). *Biophot. Int.* **11**, 36–42.
- Barberi, F., Rosi, M. & Sodi, A. (1993). *Acta Vulcanol.* **3**, 173–187.
- Baruchel, J., Buffière, J.-Y., Maire, E., Merle, P. & Peix, G. (2000). *X-ray Tomography in Material Science, General Principles*. Paris: Hermes Science.
- Behncke, B., Neri, M., Pecora, E. & Zanon, V. (2006). *Bull. Volcanol.* **69**, 149–173.
- Bertagnini, A., Métrich, N., Landi, P. & Rosi, M. (2003). *J. Geophys. Res.* **108**, 2336.
- Blower, J. D., Keating, J. P., Mader, H. M. & Phillips, J. C. (2002). *J. Volcanol. Geotherm. Res.* **120**, 1–23.
- Bouvet de Maissonneuve, C., Bachmann, O. & Burgisser, A. (2008). *Bull. Volcanol.* **71**, 643–658.
- Burton, M. R., Mader, H. M. & Polacci, M. (2007). *Earth Planet. Sci. Lett.* **264**, 46–60.
- Carroll, M. R. & Holloway, J. R. (1994). *Volatiles in Magmas*. Washington: Mineralogical Society of America.
- Cashman, K. V. & Mangan, M. T. (1994). *Volatiles in Magmas*, edited by M. R. Carroll and J. M. Holloway, pp. 447–478. Washington: Mineralogical Society of America.
- Cashman, K. V., Mangan, M. T. & Newman, S. (1994). *J. Volcanol. Geotherm. Res.* **61**, 45–68.
- Cloetens, P., Barrett, R., Baruchel, J., Guigay, J. P. & Schlenker, M. (1996). *J. Phys. D.* **29**, 133–146.
- Gaonac'h, H., Lovejoy, S., Stix, J. & Shertzer, D. (1996b). *Earth Planet. Sci. Lett.* **139**, 395–409.
- Gaonac'h, H., Stix, J. & Lovejoy, S. (1996a). *J. Volcanol. Geotherm. Res.* **74**, 131–153.
- Gualda, G. A. R. & Rivers, M. (2006). *J. Volcanol. Geotherm. Res.* **154**, 48–62.
- Gurioli, L., Harris, A. J. L., Houghton, B. F., Polacci, M. & Ripepe, M. (2008). *J. Geophys. Res.* **113**, B08206.
- Herman, G. T. (1980). *Image Reconstruction From Projections*. New York: Elsevier.
- Higgins, M. D. (2006). *Quantitative Textural Measurements in Igneous and Metamorphic Petrology*. Cambridge University Press.
- Houghton, B. F., Wilson, C. J. N., Del Carlo, P., Coltelli, M., Sable, J. E. & Carey, R. (2004). *J. Volcanol. Geotherm. Res.* **137**, 1–14.
- Jerram, D. A. & Martin, V. (2008). *Dynamics of Crustal Magma Transfer, Storage and Differentiation*, edited by C. Annen and J. F. Zellmer, pp. 133–148. London: Geological Society of London.
- Kak, A. C. & Slaney, M. (1988). *Principles of Computerized Tomographic Imaging*. New York: IEEE Press.
- Ketcham, R. A. (2005). *Geosphere*, **1**, 32–41.
- Ketcham, R. A., Meth, C., Hirsch, D. M. & Carlson, W. D. (2005). *Geosphere*, **1**, 42–59.
- Klug, C., Cashman, K. V. & Bacon, C. R. (2002). *Bull. Volcanol.* **64**, 486–501.
- Mancini, L., Montanari, F. & Dreossi, D. (2003). *Image reconstruction and analysis for X-ray computed microtomography*, Elettra Internet Report, Elettra, Trieste, Italy. (http://www.ts.infn.it/experiments/syrma/SYRMEP/Tutorial_tomo_program.ppt.)
- Mancini, L., Reiner, E., Cloetens, P., Gastaldi, J., Härtwig, J., Schlenker, M. & Baruchel, J. (1998). *Philos. Mag. A*, **78**, 1175–1194.
- Oppenheimer, C., Pyle, D. M. & Barclay, J. (2003). *Volcanic Degassing*. London: Geological Society of London.
- Piochi, M., Polacci, M., De Astis, G., Zanetti, A., Mangiacapra, A., Vannucci, R. & Giordano, D. (2008). *Geochem. Geophys. Geosyst.* **9**, Q03013.
- Polacci, M., Baker, D. R., Mancini, L., Favretto, S. & Hill, R. J. (2009). *J. Geophys. Res.* **114**, B01206.
- Polacci, M., Baker, D. R., Mancini, L., Tromba, G. & Zanini, F. (2006). *Geophys. Res. Lett.* **33**, L13312.
- Polacci, M., Papale, P. & Rosi, M. (2001). *Bull. Volcanol.* **63**, 83–97.
- Polacci, M., Pioli, L. & Rosi, M. (2003). *Bull. Volcanol.* **65**, 418–432.
- Robin, C., Eissen, J.-P. & Monzier, M. (1993). *J. Volcanol. Geotherm. Res.* **55**, 225–238.
- Rust, A. C. & Cashman, K. V. (2004). *Earth. Planet. Sci. Lett.* **228**, 93–107.
- Snigirev, A., Snigireva, I., Kohn, V., Kuznetsov, S. & Schelokov, I. (1995). *Rev Sci Instrum.* **66**, 5486–5492.
- Song, S. R., Jones, K. W., Lindquist, W. B., Dowd, B. A. & Sahagian, D. L. (2001). *Bull. Volcanol.* **63**, 252–263.
- Wright, H. M. N., Cashman, K. V., Gottesfeld, E. H. & Roberts, J. J. (2009). *Earth. Planet. Sci. Lett.* **280**, 93–104.